CRISPR screen reveals that EHEC's T3SS and Shiga toxin rely on shared host factors for infection

Alline R. Pacheco[1,2], Jacob E. Lazarus[1,2,3], Brandon Sit[1,2], Stefanie Schmieder[4,5,6], Wayne I. Lencer[4,5,6], Carlos J. Blondel[7], John G. Doench[8], Brigid M. Davis[1,2], Matthew K. Waldor[1,2,8,9*]

[1]Division of Infectious Diseases, Brigham and Women's Hospital. Boston, MA, USA

[2]Department of Microbiology and Immunobiology, Harvard Medical School. Boston, MA, USA

[3]Division of Infectious Diseases, Massachusetts General Hospital. Boston, MA, USA

[4]Division of Gastroenterology, Boston Children's Hospital. Boston, MA, USA

[5]Department of Pediatrics, Harvard Medical School. Boston, MA, USA

[6]Department of Pediatrics, Harvard Digestive Diseases Center. Boston, MA, USA

[7]Institute of Biomedical Sciences, Universidad Autónoma de Chile. Santiago, Chile

[8]Broad Institute of MIT and Harvard. Cambridge, MA, USA

[9]Howard Hughes Medical Institute, Boston, MA, USA

*To whom correspondence should be addressed.

E-mail: mwaldor@research.bwh.harvard.edu

Key words: CRISPR screen, host susceptibility, T3SS, Shiga toxin, EHEC, EPEC, sphingolipid synthesis, TM9SF2, LAPTM4A

Abstract

Enterohemorrhagic *Escherichia coli* (EHEC) has two critical virulence factors – a type III secretion system (T3SS) and Shiga toxins (Stx) – that are required for the pathogen to colonize the intestine and cause diarrheal disease. Here, we carried out a genome-wide CRISPR/Cas9 loss-of-function screen to identify host loci that facilitate EHEC infection of intestinal epithelial cells. Many of the guide RNAs identified targeted loci known to be associated with sphingolipid biosynthesis, particularly for production of globotriaosylceramide (Gb3), the Stx receptor. Two loci (TM9SF2 and LAPTM4A) with largely unknown functions were also targeted. Mutations in these loci not only rescued cells from Stx-mediated cell death, but also prevented cytotoxicity associated with the EHEC T3SS. These mutations interfered with early events associated with T3SS and Stx pathogenicity, markedly reducing entry of T3SS effectors into host cells and binding of Stx. The convergence of Stx and T3SS onto overlapping host targets provides guidance for design of new host-directed therapeutic agents to counter EHEC infection.

Importance

Enterohemorrhagic *Escherichia coli* (EHEC) has two critical virulence factors – a type III secretion system (T3SS) and Shiga toxins (Stx) – that are required for colonizing the intestine and causing diarrheal disease. We screened a genome-wide collection of CRISPR mutants derived from intestinal epithelial cells and identified mutants with enhanced survival following EHEC infection. Many had mutations that disrupted synthesis of a subset of lipids (sphingolipids) that includes the Stx receptor globotriaosylceramide (Gb3), and hence protect against Stx intoxication. Unexpectedly,

we found that sphingolipids also mediate early events associated with T3SS pathogenicity. Since antibiotics are contraindicated for the treatment of EHEC, therapeutics targeting sphingolipid biosynthesis are a promising alternative, as they could provide protection against both of the pathogen's key virulence factors.

Introduction

Enterohemorrhagic *E. coli* (EHEC) is a food-borne human pathogen that causes diarrheal illness worldwide. Infection is often associated with bloody diarrhea that is usually self-limited; however, 5-7% of cases progress to hemolytic uremic syndrome (HUS), a life-threatening complication that can result in renal failure and neurological sequelae (1). EHEC pathogenesis shares many features with that of enteropathogenic *E. coli* (EPEC), another extracellular pathogen that colonizes the intestine. Successful colonization by both species is dependent upon a type III secretion system (T3SS) that enables tight adherence of bacteria to host epithelial cells by inducing characteristic actin cytoskeletal rearrangements and loss of microvillus structure (attaching and effacing (AE) lesions) (2). EHEC virulence is also markedly shaped by production of Shiga toxins (Stx), variants of which are often present in multiple copies within the EHEC genome. Translocation of Stx to tissues outside of the intestinal tract is thought to underlie the development of HUS (3, 4).

The EHEC T3SS injects a plethora of effector proteins into host cells, resulting in alteration or disruption of numerous host cell processes. During infection, EHEC is thought to target epithelial cells within the large intestine; however, a variety of cultured

cell lines have been used to characterize the activity of this system. In vivo and in vitro studies have revealed that a key effector is the Translocated Intimin Receptor (Tir) (5). Tir is inserted into the host cell membrane and serves as a receptor for the bacterial adhesin, intimin (6). Interactions between intimin and Tir are also required for recruitment and rearrangement of actin and other cytoskeletal proteins underneath adherent bacteria, which results in characteristic actin-rich “pedestals.” In animal models, deletions of *tir* or *eae* (the intimin locus) and mutations that render the T3SS inactive markedly reduce the pathogen’s capacity to colonize the intestine and cause disease (7, 8).

Thirty eight bacterial proteins in addition to Tir have been confirmed as type 3 secreted effector proteins in EHEC (9). Unlike structural components of the T3SS, individual effector proteins are frequently not essential for bacterial virulence; although their roles have not been fully defined, it is clear that effector proteins can act in redundant, synergistic and antagonistic fashions (10). Key host processes modulated by EHEC effectors include innate immunity, cytoskeletal dynamics, host cell signaling, and apoptosis (11). EHEC effectors also restrict host cell phagocytosis of this extracellular pathogen. Effectors undergo an ordered translocation and after its translocation, the effector protein EspZ functions as a “translocation stop” that prevents unlimited effector translocation and reduces infection-associated cytotoxicity (12). Compared to wt infection, in vitro infection with *espZ*-deficient strains results in greater host cell detachment, loss of membrane potential, and formation of condensed nuclei (13).

Although Stx are pivotal to EHEC pathogenesis, the effects of these AB_5 toxins on the intestinal epithelium per se are not entirely clear. Toxicity was initially thought to be largely restricted to tissues beyond the intestinal tract (e.g., microvascular endothelial cells within the kidneys and the brain in the setting of HUS) (14); however, more recent in vivo and ex vivo studies suggest that Stx intoxication may also occur in the intestine at the primary site of infection. Although at low levels, receptors for Stx are present within human colonic epithelial cells (15), and Stx2 causes extensive cell death to the intestinal mucosa (16, 17). Furthermore, oral administration of Stx can lead to diarrhea in animals, and in several animal models of EHEC intestinal disease, severe diarrhea is dependent on Stx (8, 17).

The principal receptor for most forms of Stx (including Stx1 and Stx2, which are produced by the EHEC strain used in this study) is a neutral glycosphingolipid, globotriaosylceramide (Gb3). Following binding of Stx to Gb3, the toxin is internalized and undergoes retrograde transport through early endosomes, the Golgi, and the ER; the A subunit is cleaved by furin in the Golgi, followed by disulfide bond reduction in the ER that releases the catalytic active A1 fragment, which undergoes retro-translocation into the cytosol (18). Site specific depurination of 28S rRNA by the toxin results in inhibition of protein synthesis and can induce the ribotoxic stress response, the unfolded protein response, and apoptosis (19–22).

Analyses of EHEC pathogenesis have primarily focused upon identification and characterization of bacterial factors rather than on host factors required for

pathogenicity. Though some host factors, particularly those required for the actions of Stx and of the T3SS effectors, have been identified, to date, unbiased genome-wide screens for EHEC susceptibility loci have not been reported. Recently, such screens have become possible, given the advent of CRISPR/Cas9-based libraries of host mutants whose composition can be monitored using high throughput DNA sequencing. We recently used this approach to screen for host factors that mediate susceptibility to *V. parahaemolyticus'* two T3SS, and identified several host processes not previously linked to T3SS activity (23). The efficiency and power of this approach (24, 25), prompted us to adopt this approach to identify mutants with heightened resistance to EHEC.

Here, we identify and characterize intestinal epithelial cell mutants that become enriched following library infection with an EHEC strain producing an active T3SS as well as Stx. Although minimal overlap between the action of the T3SS and Stx have previously been reported, we identified several host loci and processes that are required for the effects of both virulence factors. Genes required for production of the Stx receptor Gb3 and other sphingolipids were also found to be necessary for translocation of T3SS effectors into host cells. Additionally, we identified 2 minimally characterized loci not previously linked to either T3SS or Stx response pathways and find that they are critical for the biogenesis of host cell Gb3 and hence susceptibility to EHEC infection.

Results

CRISPR/Cas9 screen for host factors conferring susceptibility to EHEC infection

We developed a genome-wide CRISPR/Cas9 screen to identify host factors that contribute to susceptibility to EHEC infection in the HT-29 colonic epithelial cell line using the Avana library of sgRNAs (23). This library contains four sgRNAs targeting each of the annotated human protein coding genes (26). Host cells were infected with a Δ*espZ* derivative of EHEC strain EDL933 (which carries genes encoding both Stx1 and Stx2). The Δ*espZ* mutation heightens T3SS activity and increases host cell death associated with infection by EHEC (13) (Fig. S1A). We anticipated that if we could increase the toxicity of the EHEC T3SS (Fig. S1B), we would enhance the screen's selective pressure and yield greater enrichment of host cell mutants resistant to this key virulence system. Although Stx1 and Stx2 were also produced under infection conditions (Fig. S1C), initial toxicity assays using purified toxin suggested that they would not exert substantial selective pressure during the screen. In contrast to infection of cells with Δ*espZ* EHEC, which resulted in marked (~80%) host cell death by the end of the infection period (Fig. 1AB), a corresponding 6-hour treatment of cells with purified toxin exceeding the amount detected during infection had minimal effect on viability (Fig. S1D).

For the screen, two biological replicates of libraries of HT-29 cells mutagenized with the Avana guide RNAs were infected for 6 hr with Δ*espZ* EHEC at an MOI of 100 (Fig. 1A). Following infection, resistant cells were cultured in the presence of antibiotics until reaching ~70% confluency (~5 days), then reseeded and reinfected. Genomic DNA was isolated from a fraction of the surviving population after each of the four rounds of infection as well as from the initial uninfected cells, and high throughput sequencing of

integrated sgRNA templates was performed to indirectly quantify the abundance of the associated mutants. We found that as our screen progressed, as would be expected for a library under strong selection, representation became biased toward a subset of enriched genes (Fig. S2A). Statistical analysis was performed using the STARS algorithm, which integrates data from independent guides targeting the same gene to identify the most enriched genotypes (26).

We identified 13 loci with statistically significant enrichment ($p < 0.001$) in both libraries after 4 rounds of infection (Fig. 2A). Unexpectedly, given our results with purified toxin, more than half of the enriched loci encoded factors associated with sphingolipid biosynthesis, and many were closely connected to synthesis of Gb3, the Stx receptor (Fig. 2B). For example, hits included the Golgi-localized enzymes A4GALT, which catalyzes the final step in Gb3 synthesis; B4GALT5, which catalyzes production of the A4GALT substrate lactosylceramide; and UGCG, which converts ceramide (a precursor for all glycosphingolipids) into glucosylceramide. Additional hits included the ER-localized SPTLC2, SPTSSA, and KDSR, all of which lie on the ceramide synthesis pathway, and ARF1, which indirectly regulates intracellular trafficking of glucosylceramide (27).

Enriched loci also included two genes, TM9SF2 and LAPTM4A, whose functions are largely unknown. Although both are members of larger gene families of structurally related proteins, only guide RNAs targeting these particular family members were found to be enriched, suggesting that they have specific functions conferring susceptibility to

EHEC infection (Fig. S2B). Human TM9SF2 has been reported to be a Golgi-resident transmembrane protein required for the Golgi localization of NDST1, a sulfotransferase (28). Its homologs in Drosophila (TM9SF2/4) and Dictyostelium (Phg1A/Phg1C) have been linked to innate immunity and membrane protein localization (29, 30). LAPTM4A has been reported to encode a transmembrane protein localized to lysosomes and late endosomes. It has been linked to intracellular transport of nucleosides, multidrug resistance, and maintenance of lysosomal integrity (31–34). In addition to the enrichment of guides targeting TM9SF2, LAPTM4A, and genes related to sphingolipid biosynthesis, our analysis detected enrichment for guides targeting several genes associated with cancer and cell proliferation (MLLT3, TFAP4, ZNF217, and DUSP6) (35–38).

The prominence among our hits of Gb3-related genes was unanticipated, because our preliminary studies suggested that T3SS rather than Stx would exert the strongest selective pressure in our screen. T3SS from several organisms have been hypothesized to associate with lipid rafts (39–41), transient membrane microdomains which typically are enriched in sphingolipids (including Gb3) (19); however, studies of T3SS activity and host membrane components have generally focused on the importance of cholesterol, and a role for Gb3 in EHEC pathogenesis beyond that of Stx receptor has not been reported. To more precisely define the contribution of screen hits to susceptibility to EHEC infection, we developed assays that enabled the effects of Stx and T3SS on HT-29 cells to be investigated independently. Host cells were infected in parallel with an Δ*espZ,* an Δ*espZ* Δ*escN* mutant (which lacks an ATPase essential for

T3SS activity), an Δ*espZ* Δ*stx1* Δ*stx2* mutant (ΔΔ*stx*, which does not produce Stx1 or Stx2), or mock infected, and the number of host cells present after 1 or 5 days of infection was determined (Fig. S1B). These experiments revealed similar marked declines in abundance of HT-29 cells 1 day post-infection with the type 3-active Δ*espZ* or Δ*espZ* ΔΔstx EHEC (to <20% of that seen in mock infected cells; Fig. 1B); in contrast the type 3-deficient but toxin-producing Δ*espZ* Δ*escN* infection had no significant effect on host cell abundance at this time point (Fig. 1B). However, in the subsequent 4 days, there was a marked difference in growth between cells infected with the Δ*espZ* vs. Δ*espZ* ΔΔ*stx* strains. Population expansion of cells previously exposed to toxin (Δ*espZ* infection*)* was far slower than that of cells that were never exposed to the toxin (Δ*espZ* ΔΔ*stx* infection) (Fig. 1C, Fig. S1B). The abundance of HT-29 cells infected with the Δ*espZ*Δ *escN* strain also differed significantly from that of mock infected cells by day 5, likely further reflecting the consequence of toxin exposure at this time point. Collectively, these analyses demonstrate that the impact of T3SS is most clearly evident 1 day post infection, and can be differentiated from that of toxin via infection with the Δ*espZ* ΔΔ*stx* strain. In contrast, the effects of Stx are delayed and become more apparent 5 days post infection, and can be assayed in infection with the T3SS-deficient Δ*espZ* Δ*escN* strain. Given that our screen included multiple rounds of 5-day outgrowth following infection (during which effects of Stx could manifest), we conclude that the screen enriched for mutants resistant to Stx as well as T3SS.

For initial validation of our screen hits, mutants corresponding to selected enriched loci were constructed and verified by Sanger sequencing or Western blot (Fig. S2C-E), and

231 their abundance (relative to mock infected cells) was assessed 5 days post-infection
232 with Δ*espZ* EHEC. In comparison to the HT-29 Cas9 control strain, all but one mutant
233 (ARF1) had significantly enhanced abundance at 5 days post-infection (Fig. 2C),
234 suggesting that our selection and analysis yielded robust and reliable data regarding
235 susceptibility to EHEC infection.
236
237 **Sphingolipid biosynthesis facilitates T3SS killing**
238 Because the hits predicted to be involved in cell proliferation (i.e. DUSP6, TFAP4,
239 ZNF217 and MLLT3) were less likely to be involved in EHEC pathogenesis per se, we
240 chose to focus further studies on a subset of the sphingolipid biosynthesis mutants and
241 on mutants in the largely uncharacterized loci TM9SF2 and LAPTM4A. In particular, we
242 focused on factors mediating synthesis of glycosphingolipids, particularly A4GALT,
243 which should only have impaired production of Gb3 and other globo-series
244 glycosphingolipids (42), and UGCG, which is required for synthesis of all
245 glycosphingolipids except galactosylceramines (43). ARF1 was also included, due to its
246 contribution to intracellular trafficking of UGCG's product from the cis-medial Golgi to
247 the trans Golgi network, where B4GALT5 and A4GALT are found (44). To assess the
248 bacterial factors underlying the enrichment of these loci, mutants were first infected with
249 the Δ*espZ* ΔΔ*stx* strain or mock infected, and cell abundance was assessed one day
250 following infection. Notably, all of the mutant cells displayed significantly elevated
251 relative abundance compared to wt HT-29 cells (Fig. 3A). Coupled with our prior
252 analyses of bacterial factors modulating host survival at this time point (Fig. 1B), these
253 results suggest that these mutations confer resistance to Δ*espZ* ΔΔ*stx* infection by

protecting against the effects of EHEC's T3SS, and thus that associated loci may play a role in the host cell response to T3SS. Of these factors, only ARF1 has previously been linked to T3SS-mediated processes; it is thought to facilitate insertion of the T3SS translocon during Yersinia infection (45) but has not been linked to T3SS activity in EHEC.

The first effector translocated by EHEC's T3SS – Tir – is essential for the activity of this secretion system. In the absence of Tir, translocation of additional effectors does not occur, nor does the characteristic cytoskeletal rearrangement and formation of membrane "pedestals" underneath adherent bacteria (5, 46). Tir translocation can be assessed using a Tir-CyaA reporter fusion protein, followed by measurement of intracellular cAMP levels (47). We monitored translocation of this reporter, which is dependent on an intact T3SS, from wt EHEC into control HT-29 Cas9 cells and mutants that appeared resistant to the effects of T3SS. These experiments revealed significantly lower Tir translocation into all mutants than into control HT-29 cells, ranging from ~70% (A4GALT) down to ~10% (LAPTM4A) of wt levels (Fig. 3B). Consistent with this observation, immunofluorescence microscopy of wt and mutant HT-29 cells infected with wt EHEC revealed markedly fewer adherent bacteria and associated actin-rich pedestals. While EHEC formed pedestals on ~80% of infected wt HT-29 cells, pedestals were detected on only 18-35% of infected mutants tested, and fewer pedestals were generally observed per mutant cell (Fig. 3CDE, Fig. S3A). Collectively, these results indicate that the mutations rendering HT-29 cells less susceptible to the cytotoxic effects of EHECs T3SS all limit early steps in the T3SS effector translocation process,

277 although they do not fully disrupt this process. These results also demonstrate that the
278 mutants identified in our screen are protective against EHEC even when its T3SS
279 activity has not been augmented by mutation of Δ*espZ*.
280
281 EHEC's T3SS machinery and associated effectors are similar to those of
282 enteropathogenic *E. coli* (EPEC), a related pathogen that does not produce Shiga toxin
283 but that also requires its T3SS to colonize and cause disease in the human intestine
284 (48). We investigated whether the mutations that protect HT-29 cells from EHEC
285 infection also render HT-29 less susceptible to EPEC. Wt and mutant HT-29 cells were
286 infected with an EPEC Δ*espZ* mutant that, like its EHEC counterpart, is reported to have
287 increased cytotoxicity relative to the wt strain (13, 49) (Fig. S3B). All 5 mutants tested
288 exhibited increased survival compared to the wt cells at 1 day post infection, and this
289 increase was linked to the presence of a functional T3SS (Fig. S3C). Survival of the
290 TM9SF2 and ARF1 mutants was particularly enhanced, with the number of infected
291 cells nearing 50% of the mock infected controls, compared to the ~5% observed with wt
292 HT-29. Overall, our observations suggest that host glycosphingolipids modulate T3SS-
293 mediated cytotoxicity for both pathogens, although pathogen reliance on particular
294 sphingolipids is not necessarily conserved. For example, the absence of A4GALT had a
295 dramatic effect on EHEC cytotoxicity, but only a modest influence on EPEC cytotoxicity.
296 Additionally, our results suggest that TM9SF2 may play a conserved role in facilitating
297 the activity of the EHEC and EPEC T3SS.
298

Given previous reports that lipid rafts may promote T3SS activity, that Gb3 high-density association within lipid rafts is important for Stx binding (50), and our screen's identification of numerous sphingolipid-related loci, we hypothesized that TM9SF2 and LAPTM4A mutants might be less susceptible to EHEC infection due to alterations in lipid raft production or dynamics. To explore these possibilities, we compared the trafficking in control, TM9SF2 and LAPTM4A cells of a chimeric GPI-anchored GFP construct (GPI-GFP), which is transported to the plasma membrane where it becomes enriched in lipid rafts (51). Cell surface fluorescence was similarly homogenous in all three genetic backgrounds, and we could not detect consistent differences in steady state plasma membrane fluorescence between the 3 samples (Fig. S3D). To determine if kinetics of trafficking and insertion might nevertheless differ between wt and mutant cells, we performed quantitative photobleaching. The rate of signal decay was similar for all 3 backgrounds, suggesting that bulk plasma membrane trafficking and lipid raft insertion is not grossly disrupted in TM9SF2 and LAPTM4A cells (Fig. S3E). Further studies will be needed to define the precise means by which these mutations, as well as others tested above, limit susceptibility to EHEC and EPEC's T3SS.

LAPTM4A and TM9SF2 are required for Gb3 biosynthesis

As noted above, the effects of Stx on HT-29 abundance were evident 5 days post-infection, and could be clearly distinguished from those of EHEC's T3SS through infection with the Stx+ T3SS-deficient Δ*escN* mutant (Fig. 1C). Therefore, we also compared the abundance of wt HT-29 cells and several mutants from our panel after challenge with the Δ*escN* strain. As anticipated, mutants lacking the sphingolipid

biosynthesis factors A4GALT, UGCG, and SPTLC2 (all of which contribute to Gb3 production) were far less susceptible to Δ*escN* infection than wt HT-29 cells; at 5 days post infection, the abundance of these mutants did not differ from that of mock-infected controls (Fig. 4A). Intriguingly, the TM9SF2 and LAPTM4A mutants were also significantly more abundant than wt cells by 5 days post Δ*escN* infection, suggesting that these factors not only contribute to resistance to T3SS-mediated cytotoxicity, but also could be host factors facilitating intoxication.

To begin to explore the means by which TM9SF2 and LAPTM4A mutations protect against Stx, we tested the capacity of mutants to bind to fluorescently tagged toxin. As controls, we also assayed A4GALT and UGCG mutants, which are known to be completely deficient in Gb3 production, and hence cannot bind Stx. Flow cytometry analyses, which were performed both in HT-29 (Fig. 4B) and HeLa (Fig. S4A) cells, revealed that there was a high (but not uniform) level of binding of Stx2 to both wt cell types. Notably, there was marked reduction in Stx binding in both the TM9SF2 and LAPTM4A mutant cells (Fig. 4B and Fig. S4A); these mutants bound equal to or less toxin than the A4GALT and UGCC mutants. The residual binding observed in all genetic backgrounds may reflect non-specific toxin adsorption or low level genetic heterogeneity in the CRISPR/Cas9-mutagenized lines.

Similarly, fluorescence microscopy, which was performed using wt HeLa cells and their derivatives due to their favorable imaging characteristics, did not reveal Stx binding to any of the mutants, even when cells were permeabilized to enable binding to

intracellular receptor (Fig. 4C, D). Thus, the TM9SF2 and LAPTM4A mutants' deficiencies in Stx binding do not appear to reflect impaired trafficking of Gb3 to the cell surface, but instead reflect defective synthesis and/or enhanced degradation of this glycosphingolipid.

To evaluate the specificity of the deficiency in the TM9SF2 and LAPTM4A HT-29 mutants, we used flow cytometry to measure their capacity to bind cholera toxin (CT), which interacts with the glycosphingolipid GM1 (Fig. 2B) (52). In contrast to the near ablation of Stx binding in these mutants, there was a comparatively modest reduction in the binding of fluorescently labeled CT to these cells compared to wt HT-29 cells and A4GALT mutant cells (which produce normal amounts of GM1) (Fig. S4B). As expected, the UGCG cells showed a far more marked decrease in binding to cholera toxin, since UGCG is required for synthesis of GM1 (43). Collectively, these observations suggest that the TM9SF2 and LAPTM4A mutants' deficiencies in Stx binding reflect relatively specific reductions in production of Gb3 or related globo-series glycosphingolipids, rather than deficiencies that consistently impair synthesis or trafficking to the cell membrane of multiple surface receptors. Coupled with our analysis of the set of mutants that display reduced sensitivity to T3SS-mediated cytotoxicity, these observations suggest that reduced production of Gb3 likely contributes to the TM9SF2 and LAPTM4A mutants' resistance to the effects of EHEC's T3SS as well as to Stx.

To gain greater insight into the mechanism by which TM9SF2 and LAPTM4A enable infection by EHEC, we determined their subcellular localization in HeLa cells via

confocal microscopy. Consistent with previous reports (28), we found that TM9SF2 co-localized with GM130, a Golgi matrix protein (Fig. 5A). A subset of fluorescence emanated from nucleoli, potentially resulting from non-specific primary antibody binding, though Stx has been reported to be actively transported into nucleoli (53). Unexpectedly, as prior studies localized LAPTM4A to lysosomes (31-34), we found that a LAPTM4A-GFP fusion protein localized to the Golgi, like TM9SF2 (Fig. 5A).

The subcellular distribution of TM9SF2 and LAPTM4A raised the possibility that these proteins might enable EHEC infection by facilitating Gb3 biosynthesis, either by participating in Golgi-localization of precursor substrates or enzymes specifically, or by acting more generally as matrix proteins to ensure overall Golgi integrity. To investigate the former possibility, we immunolabeled the A4GALT enzyme in wt and in TM9SF2 and LAPTM4A cells. A4GALT maintained proper Golgi localization in both mutant cell lines (Fig. 5B), suggesting that TM9SF2 and LAPTM4A are not required either for the production or distribution of A4GALT. To investigate if TM9SF2 and LAPTM4A might instead facilitate Gb3 trafficking by acting more generally in Golgi integrity, we performed qualitative and quantitative image analysis of both cis-medial- and trans-Golgi compartments. GM130 (a cis-medial Golgi marker) appeared morphologically normal in the mutant cells (Fig. S5A) and quantitative characterization of the trans-Golgi, where the final step in Gb3 biosynthesis is thought to occur, did not reveal differences in either the integrity (as measured by confocal Z-stack nominal 2-dimensional area) or localization (as measured by nuclear centroid displacement) of this

sub-compartment (Fig. S5BC). Further analyses will be required to identify the precise defect that leads to glycosphingolipid deficiency in these mutants.

Discussion

EHEC encodes two potent virulence factors that empower it to disrupt the colonic epithelium during infection: its T3SS, which enables intimate attachment of bacteria as well as translocation of multiple effectors that disrupt epithelial cell processes, and Stx, a potent translation inhibitor that triggers multiple stress responses in cells within and outside of the intestinal tract. These virulence factors were acquired by horizontal transmission in distinct steps in the pathogen's evolution (54) and are generally thought of as functionally independent. However, our CRISPR/Cas9-based screen for host mutants with reduced susceptibility to EHEC infection uncovered a remarkable overlap in host factors that mediate the response to these bacterial products. The screen for mutations enriched after infection with Stx+ and T3SS+ EHEC identified numerous loci known to be associated with sphingolipid and glycosphingolipid biosynthesis, in particular factors required for production of the Stx receptor Gb3, as well as two loci (TM9SF2 and LAPTM4A) with largely undefined cellular roles that were also required for toxin binding. Unexpectedly, mutants lacking these factors are also less susceptible to cytotoxicity associated with EHECs T3SS. These mutations interfered with early events associated with T3SS and Stx pathogenicity, markedly reducing entry of T3SS effectors into host cells and binding of Stx. Although the means by which these host loci and the processes associated with them are exploited by EHEC are not fully

understood, the convergence of Stx and T3SS onto overlapping targets raises intriguing possibilities for design of therapeutic agents countering EHEC infection.

Previous studies of Stx and EHEC T3SS have characterized some of the pathways through which these factors act upon host cells, such as the binding and retrograde transport that enables Stx to reach its intracellular target, the stress responses induced by Stx, the processes underlying formation of pedestals, and the targets and mechanisms of effectors (55–58). Notably, our findings suggest that disruption of only a subset of host genes provides protection against cytotoxicity when both virulence factors are present. Interestingly, we identified loci that influence early steps within virulence pathways, e.g., loci that are required for Stx binding to host cells or T3SS effector translocation rather than loci that mediate toxin trafficking (e.g., clathrin, dynamin, SNX1/2) (18) or interact with translocated effectors (e.g., N-WASP, IRTKS, IRSp53) (58–60). Such proximal factors have also been identified in other genome-wide CRISPR screens for host mutants resistant to cytotoxicity by other pathogens. For example, a Yersinia RNAi screen and our *Vibrio parahaemolyticus* CRISPR screen yielded loci that reduced effector translocation (23, 45). For EHEC virulence factors, disrupting early steps in their interactions with host cells may be particularly protective because these virulence factors disrupt multiple cellular processes once internalized; for example, inactivation of the host response to a single T3SS effector may still leave cells vulnerable to the activity of other growth-interfering effectors.

Early steps in the interactions between host cells and EHEC's virulence factors were also likely identified in our screen because of the previously unrecognized overlap between host factors utilized by T3SS and Stx at the start of their encounters with epithelial cells. We found that mutants with disrupted synthesis of Gb3, which were expected to be resistant to Stx-mediated growth inhibition, also exhibited an unexpected reduction in their sensitivity to T3SS-mediated cytotoxicity that was associated with reduced translocation of Tir. A majority of these mutants also exhibited reduced susceptibility to EPEC infection, suggesting that common host processes may mediate the actions of EHEC and EPEC's related T3SS.

Although many mutants identified by our screen share the characteristic of lacking Gb3, it is unlikely that this deficit is the sole factor underlying their resistance to T3SS. Mutants lacking A4GALT, UGCG, TM9SF2 and LAPTM4A appear equally devoid of extracellular Gb3 in assays of Stx binding; however, they exhibit varying degrees of resistance to Δ*espZ* EHEC. T3SS resistance is also not fully correlated with the extent to which Tir translocation into these cells is reduced. These observations suggest that the reduction in Gb3 levels is associated with additional cellular changes (e.g., in overall sphingolipid homeostasis, membrane/lipid raft composition, or intracellular trafficking) that also modulate the host response to EHEC infection.

The means by which mutations in TM9SF2 and LAPTM4A prevent accumulation of Gb3 remain to be determined. We found that both proteins are localized within the Golgi, raising the possibility that they modulate the activity, localization, or transport of

457 glycosphingolipid biosynthetic factors, which also occurs within this organelle. TM9SF2
458 was previously found to regulate the localization of NDST1, a Golgi localized enzyme
459 that catalyzes N-sulfation of heparan sulfate, and to be required for accumulation of
460 NDST1's reaction product (28). TM9SF2 and the associated heparan sulfate N-sulfation
461 are important for host cell binding and entry by CHIKV virus (28); however, the absence
462 of other hits associated with heparan sulfate in our screen suggests that this phenotype
463 is not related to our results. Minor abnormalities in several other glycosylation pathways
464 were also associated with TM9SF2 disruption, but the underlying mechanism was not
465 determined. We found that TM9SF2 is not required for correct localization or
466 accumulation of A4GALT, suggesting that TM9SF2 may act prior to the terminal step of
467 Gb3 synthesis. Similarly, LAPTM4A mutation did not appear to modulate A4GALT
468 production or localization. It is unclear why previous studies have observed LAPTM4A
469 in lysosomes and late endosomes rather than the Golgi localization that we detected;
470 further studies will be needed to dissect the targeting and activity of LAPTM4A and its
471 relationship to production of Gb3. Protein annotation and studies in the mouse homolog
472 (MTP) suggest LAPTM4A may be involved in intracellular transport of nucleosides (61).
473 Together with its Golgi localization shown herein, LAPTM4A could be involved in
474 transporting activated sugars to the Golgi lumen, to supply precursors for Gb3
475 biosynthesis.
476
477 Although EHEC is susceptible to common antibiotics, antibiotic treatment is generally
478 contraindicated during EHEC infection, as antibiotics can increase production and
479 release of Stx, leading to the development of HUS (62). A variety of alternative

480 therapies have been proposed to counter the effects of toxin, including compounds that
481 sequester or neutralize toxin, block its binding to host cells, or disrupt toxin
482 internalization, processing, or intracellular activity (63). Their activity has largely been
483 tested in toxin-treated cell lines; a few have also been studied in animal models, but not
484 in the context of EHEC infection. Our results suggest that a subset of these compounds,
485 namely those that alter production of Gb3, may reduce pathogenesis associated with
486 T3SS as well as Stx, and thus may be particularly effective in countering EHEC
487 infection. Further studies of these and related compounds may enable identification of
488 agents that counter host susceptibility to translocation of EHEC's T3SS effectors as well
489 as to the effects of Stx, which could hold high therapeutic potential. Thus, our
490 identification of host factors related to both T3SS and Stx susceptibility provides
491 guidance in prioritizing the development of therapeutics aimed at countering EHEC
492 pathogenesis.
493

494 ## Materials and Methods

495 ### Bacterial strains, plasmids and growth conditions

496 All bacterial strains and plasmids used in this study are listed in Table S1. Primers used
497 in strain construction are shown in Table S1. Bacterial strains were cultured in LB
498 medium or on LB agar plates at 37°C unless otherwise specified. Antibiotics and
499 supplements were used at the following concentrations: carbenicillin: 50µg/ml;
500 ampicillin: 100ug/mL; chloramphenicol: 20µg/ml; kanamycin: 50µg/ml; streptomycin:
501 200µg /ml; IPTG: 1ug/ml. The EHEC Δ*espZ* deletion mutant was constructed by allelic
502 exchange using a derivative of the suicide vector pDM4 that included *espZ*-flanking

503 sequences (64). Deletion of *stx1*, *stx2* and *escN* was performed using lambda-red
504 mediated recombination (65).

505 **Eukaryotic cell lines and growth conditions**

506 HT-29, HeLa and 293T cells and their derivatives were cultured in DMEM supplemented
507 with 10% fetal bovine serum. Cells were grown at 37°C with 5% CO2 and routinely
508 passaged at 70-80% confluency; media was replenished every 2-3 days.

509 **Positive selection screen using the HT-29 CRISPR AVANA libraries**

510 The HT-29 libraries were constructed as described (23) using the AVANA sgRNA
511 library, which contains four sgRNAs targeting each of the human protein coding genes
512 (26). For each library, two sets of 7 T225 flasks were seeded with $12.5*10^6$ cells per
513 flask, then incubated for 48 hours. At the time of the screen there were $175*10^6$ cells
514 per experimental condition, corresponding to ~2000X coverage per perturbation. Cells
515 were at ~70% confluency at the time of infection. One set of flasks served as an
516 uninfected control; the second was infected with the EHEC Δ*espZ* strain. Cells were
517 harvested from the control at the time of infection.
518
519 For infection, the Δ*espZ* strain was grown overnight statically in LB media to an OD_{600nm}
520 of 0.6, then centrifuged and resuspended at OD_{600nm} 0.5 in DMEM. HT-29 cells were
521 infected with EHEC Δ*espZ* at an MOI=100 and incubated under standard culture
522 conditions for 6 hours, with a media change at 3 hr post-infection to remove
523 nonadherent bacteria and prevent media acidification. At 6-hour post-infection, cells
524 were washed 3 times with 1X DPBS to remove nonadherent bacteria, then replenished

525 with fresh media supplemented with 1X antibiotic-antimycotic solution (ABAM) (Gibco-
526 containing 100ug/mL streptomycin) and gentamicin 100ug/ml (Gent) ("stop medium").
527 After overnight incubation, fresh "stop medium" was added to each flask. Flasks were
528 monitored daily by inverted light microscopy to follow the recovery of survivor cells.
529 Upon reaching 70% confluency, the cells were trypsinized, pooled and re-seeded for the
530 next round of infection, always keeping a minimum number of $80*10^6$ cells to maintain a
531 coverage of at least 1000X. The infection and selection procedure was repeated for the
532 second, third and fourth rounds of infection. Additionally, a subset of cells from each
533 population were used for preparation of genomic DNA.
534
535 **Genomic DNA preparation, sequencing and STARS analyses of screen results**
536 Genomic DNA (gDNA) was extracted from $100x10^6$ input cells (uninfected) and after
537 each round of infection with EHEC Δ*espZ* (rounds 1, 2, 3 and 4) using the Blood and
538 Cell Culture DNA Maxi Kit from Qiagen. The gDNA was subjected to PCR to amplify
539 guide RNA sequences as previously described (26). The read counts were first
540 normalized to reads per million within each condition by the following formula: reads per
541 sgRNA/total reads per condition × 10^6. Reads per million were then log2-transformed by
542 first adding 1 to all values, in order to take the log of sgRNAs with zero reads. For
543 analyses, the log2 fold-change of each sgRNA was determined relative to the input
544 sample for each biological replicate (Table S2). The STARS algorithm for CRISPR-
545 based genetic perturbation screens was used to evaluate the rank and statistical
546 significance of the candidate genes as described (26).
547

548 **Construction of HT-29 Cas9 and HeLa cells with targeted gene disruptions**

549 The sgRNA sequences used for construction of HT-29 Cas9 mutant cells are shown in
550 Table S3. All sgRNA oligo sequences were obtained from Integrated DNA Technologies
551 and cloned into the pLentiGuide-Puro plasmid as previously described (23). Briefly, 5µg
552 of plasmid pLentiGuide-Puro was digested with *BmsBI* (Fermentas) and purified using
553 the QIAquick Gel extraction kit. Each pair of oligos was annealed and phosphorylated
554 with T4 PNK (NEB) in the presence of 10X T4 DNA ligase buffer in a thermocycler with
555 the following parameters: i) incubation for 30 minutes at 37°C, ii) incubation at 95°C for
556 5 min with a ramp down to 25°C at 5°C per minute. Oligos were then diluted 1:200 and
557 1µl of the diluted oligo mixture was ligated with 50ng of *BsmBI* digested plasmid.
558 Ligations were transformed into STBL3 bacteria, and transformed clones were checked
559 by PCR and DNA sequencing. sgRNAs cloned into pLentiGuide-Puro were transduced
560 into HT-29 Cas9 cells as described below, and after 10 days of selection with
561 Puromycin (1µg/ml), the extent of disruption of the targeted gene was analyzed by
562 immunoblotting for the corresponding gene product or Sanger sequencing (Fig. S2C).

563 **Lentivirus Preparation and Transductions**

564 Lentiviral transductions were performed as previously described (23). Briefly, all
565 lentiviruses were made by transfecting 293T cells using TransIT-LT1 transfection
566 reagent, the lentiviral packaging plasmids psPAX2 and pCMV-VSVG and the
567 corresponding cargo plasmid according to the manufacturer's protocol. 48h following
568 transfection, 293T culture supernatant was harvested, filtered through a 0.22µm pore
569 filter, and added to target HT-29 or HeLa cells grown to 70-80% confluency in 6-well
570 plates; a second virus supernatant were harvested 72 hr after transfection and added to

target cells. After each virus' supernatant addition to HT-29 cells, spin infection was performed by adding 8µg/ml polybrene and spinning the 6-well plates were at 1600g for 2h at 30°C; HT-29 cells were then returned to 37°C. Puromycin selection for positive transductants was initiated the following day. For transduction of HeLa cells, spin infection was not performed.

Cell survival assays

For cell survival assays, $5x10^5$ HT-29 cells were seeded into 6-well plates and grown for 48 hours in DMEM supplemented with 10% FBS. EHEC (or EPEC) strains for infections were prepared as for library infections described above. HT-29 cells were infected at an MOI=100 (or with uninoculated media in the case of mock infection), with media changes and infection termination as for library infection. Mock infected cells were fed but not passaged during the outgrowth period. Following infection and outgrowth for 1 or 5 days, cells were quantified by Trypan Blue (0.4%trypan blue) exclusion using a Countess II Automated Cell Counter (Thermo Fisher Scientific). Cell survival after EPEC infection was measured 4 hr post-infection.

Stx cytotoxicity assay and measurement of Stx released during infection

HT-29 cells were seeded at $1x10^6$ cells/ well the day before the assay. Cell monolayers were then exposed to a range of concentrations of pure Stx1 or Stx2 holotoxins for 6 hours. Cell survival was measured by Trypan Blue exclusion as described above, then % of survival was calculated in comparison to HT-29 controls that did not receive toxin

593 treatment. Stx released during infection of HT-29 cells at 3hr and 6hr was measured by
594 ELISA, as described (66).
595
596 **Tir Translocation Assays**
597 The Tir translocation assay was performed as previously described (47). Briefly: HT-29
598 cells were plated at $1x10^5$ cells/well in 96 wells and assayed at confluency. EHEC
599 strains harboring Tir-CyaA fusion or CyaA vector control were grown in LB overnight
600 then diluted 1:100 in DMEM and grown to OD600 = 0.6 shaking at 37C. Cells were
601 infected with MOI 100:1 for 90 minutes; cAMP was measured by ELISA using Biotrack
602 cAMP kit (Amersham) according to manufacturer's instructions.
603
604 **Immunoblot analyses**
605 Mammalian cell lysates were prepared with RIPA buffer and protein concentrations
606 were determined using BCA protein assay. 10ug of protein lysate was mixed with
607 NuPAGE LDS sample buffer (Invitrogen) with 50mM DTT, separated by NuPAGE Bis-
608 Tris gel electrophoresis and transferred to nitrocellulose membranes. Antibodies and
609 concentrations used are listed in KEY RESOURCES TABLE. Blots were developed with
610 the SuperSignal West Pico ECL kit, and imaging was performed on the Chemidoc
611 Touch Imaging System (Biorad).

612 **Immunofluorescence**
613 HT-29 cells or HeLa cells were seeded in 12-well plates on 18mm glass coverslips or 4-
614 well chambers (Mat-TEK). Cells were fixed with 2% paraformaldehyde (PFA) for 20
615 minutes at room temperature, washed with 1X PBS 3 times, then permeabilized with

616 0.1% Triton X-100 in PBS for 30 minutes (except for cells stained for TM9SF2, which
617 were subjected to combined fixation and permeabilization in ice cold methanol for 10
618 minutes). Cells were blocked in 5% normal goat serum in PBS (blocking buffer) for 1
619 hour, followed by overnight incubation with primary antibodies (Table S4) at 4°C. Cells
620 were then washed 3 times with PBS followed by incubation with fluorescently-labeled
621 secondary antibody for 1 hour at room temperature. Cells were counterstained with
622 Alexa-568 Phalloidin and DAPI for actin cytoskeleton and nuclei, respectively. For
623 extracellular binding of Alexa-488-tagged Stx, cells were not permeabilized; for
624 intracellular binding, cells were permeabilized and stained as described above.
625
626 **LAPTM4A subcellular localization**
627 HeLa Cas9 cells were plated on coverslip and transfected with LAPTM4A-GFP
628 (Origene) per the manufacturer's protocol (Mirus). 24 hours later, cells were processed
629 for immunofluorescence as above. GFP was imaged directly without additional signal
630 amplification.
631
632 **Fluorescent actin staining (FAS)**
633 FAS assays were performed as described (67) with minor modifications. Briefly, HT29
634 cells were seeded at $1x10^6$ cell/well in 4-well chambers in DMEM + FBS. Three days
635 after confluency, cells were infected with EHEC strains expressing GFP at an MOI=100
636 for 6 hours, with a media change after 3hr. After infection, cells were washed three
637 times with PBS, fixed with 2% PFA and permeabilized with 0.2% Triton X-100. Cells
638 were then stained with Alexa-633 Phalloidin and DAPI for visualization of actin

cytoskeleton and cell nuclei. Slides were mounted using Prolong Diamond Antifade and analyzed by confocal microscopy. The experiment was repeated at least 3 times, and 250 cells were counted in total. The percentage of infected cells was determined by analyzing at least 20 random fields across different experiments; numbers of pedestals were determined by counting AE lesion in 100 infected cells. All comparisons were relative to HT-29 cells.

Lipid raft assay

For imaging of GFP-GPI, the indicated cells were split into 12-well glass bottom plates (MatTek). 1 day later, cells were transfected with GFP-GPI using TransIT-LT1 reagent following the manufacturer's recommended protocol (Mirus). 24 hours later, cells were washed and then imaged in FluoroBrite-DMEM (Invitrogen), with live fields of single confocal slices of cell bottoms taken for 1 minute using 1 second exposures at 75% laser power. ROI mean intensities (with ROI drawn to avoid overlapping cell protrusions and saturated pixels) were calculated for each frame using the Plot Z-axis profile function in ImageJ. Greater than 20 cells and at least 20 movies were analyzed for each condition. Results are expressed as mean +/- SEM.

Golgi complex morphological analyses

Golgi integrity was assayed by calculation of the mean distance between the manually defined weighted centroid of nucleus (as defined by DAPI staining) and trans-Golgi (as defined by TGN46 staining), and from 2-dimensional area of manually defined ROI of

maximum-intensity projection of individual confocal slices of TGN46 staining. At least 20 cells were analyzed for each condition. Results are expressed as mean +-SEM.

Shiga toxin labeling and Flow Cytometry (FACS)

Shiga toxins 1 and 2 (holotoxins) were obtained from Tufts Medical Center; cholera toxin was purchased from Sigma. All toxins were diluted in PBS and labeled with Alexa488 or Alexa647 micro-labeling kit (Invitrogen) according to manufacturer's instructions. For FACS analysis of Stx binding, HT-29 cells were seeded at $5x10^5$ cells/well in 6-well plates, while HeLa cells were seeded $2.5x10^5$ cells/well, then incubated for 24 hours. Cell monolayers were washed 3 times with EBSS, trypsinized, resuspended in PBS with labeled Stx (10nM) or CT (1nM), and incubated on ice for 30 min. Cells were then centrifuged, resuspended in FACS buffer (DPBS + 10% FBS) and analyzed by flow cytometry.

Statistical Methods

Statistical analyses were carried out using a one-way ANOVA with Dunnet post-correction on GraphPad Prism5.

Acknowledgements

We gratefully acknowledge Professor James Kaper (University of Maryland) for providing EPEC strains and the Tir-cyaA plasmid, to Professor Yusuke Maeda (Osaka University) for providing anti-TM9SF2 antibody and to Professor Peter Howley for HeLa Cas9 parental cells. We thank Waldor lab members for helpful discussion about this

project. This work was supported by HHMI and R37 AI-042347 (MKW), B.S. was supported by National Sciences and Engineering Research Council of Canada (NSERC) PGS-D award (487259), J.E.L. was supported by the NIH under NRSA T32AI007061 from the NIAID.

References

1. Kaper JB, Brien ADO (2014) Overview and Historical Perspectives. 1–9.
2. Jarvis KG, et al. (1995) Enteropathogenic Escherichia coli contains a putative type III secretion system necessary for the export of proteins involved in attaching and effacing lesion formation. 92(August):7996–8000.
3. Dettmar AK, et al. (2014) Protection of Human Podocytes from Shiga Toxin 2-Induced Phosphorylation of Mitogen-Activated Protein Kinases and Apoptosis by Human Serum Amyloid P Component. 82(5):1872–1879.
4. Strockbine NA, et al. (1986) Two toxin-converting phages from Escherichia coli O157:H7 strain 933 encode antigenically distinct toxins with similar biologic activities. *Infect Immun* 53(1):135–140.
5. Kenny B, et al. (1997) Enteropathogenic E. coli (EPEC) transfers its receptor for intimate adherence into mammalian cells. *Cell* 91(4):511–520.
6. Jerse AE, Yu J, Tall BD, Kaper JB (1990) A genetic locus of enteropathogenic Escherichia coli necessary for the production of attaching and effacing lesions on tissue culture cells. *Proc Natl Acad Sci U S A* 87(20):7839–7843.
7. Tzipori S, et al. (1995) The role of the eaeA gene in diarrhea and neurological complications in a gnotobiotic piglet model of enterohemorrhagic Escherichia coli

706 infection. *Infect Immun* 63(9):3621–3627.

707 8. Ritchie JM, Thorpe CM, Rogers AB, Waldor MK (2003) Critical roles for stx2, eae,
708 and tir in enterohemorrhagic Escherichia coli-induced diarrhea and intestinal
709 inflammation in infant rabbits. *Infect Immun* 71(12):7129–7139.

710 9. Tobe T, et al. (2006) An extensive repertoire of type III secretion effectors in
711 Escherichia coli O157 and the role of lambdoid phages in their dissemination.
712 *Proc Natl Acad Sci U S A* 103(40):14941–14946.

713 10. Stevens MP, Frankel GADM (2014) The Locus of Enterocyte E ff acement and
714 Associated Virulence Factors of Enterohemorrhagic Escherichia coli. *Microbiol*
715 *Spectr* 2(4):1–25.

716 11. Santos AS, Finlay BB (2015) Bringing down the host: Enteropathogenic and
717 enterohaemorrhagic Escherichia coli effector-mediated subversion of host innate
718 immune pathways. *Cell Microbiol* 17(3):318–332.

719 12. Mills E, Baruch K, Charpentier X, Kobi S, Rosenshine I (2008) Real-Time Analysis
720 of Effector Translocation by the Type III Secretion System of Enteropathogenic
721 Escherichia coli. *Cell Host Microbe* 3(2):104–113.

722 13. Berger CN, et al. (2012) EspZ of enteropathogenic and enterohemorrhagic
723 Escherichia coli regulates type III secretion system protein translocation. *MBio*
724 3(5). doi:10.1128/mBio.00317-12.

725 14. Steil D, et al. (2015) Shiga toxin glycosphingolipid receptors of Vero-B4 kidney
726 epithelial cells and their membrane microdomain lipid environment. *J Lipid Res*
727 56(12):2322–2336.

728 15. Zumbrun SD, et al. (2010) Human intestinal tissue and cultured colonic cells

729 contain globotriaosylceramide synthase mRNA and the alternate shiga toxin
730 receptor globotetraosylceramide. *Infect Immun* 78(11):4488–4499.
731 16. Békássy ZD, et al. (2011) Intestinal damage in enterohemorrhagic Escherichia
732 coli infection. *Pediatr Nephrol* 26(11):2059–2071.
733 17. Stone SM, et al. (2012) Shiga toxin 2-induced intestinal pathology in infant rabbits
734 is A-subunit dependent and responsive to the tyrosine kinase and potential ZAK
735 inhibitor imatinib. 2(November):1–11.
736 18. Johannes L, Romer W (2010) Shiga toxins--from cell biology to biomedical
737 applications. *Nat Rev Microbiol* 8(2):105–116.
738 19. Kouzel IU, et al. (2013) Association of Shiga toxin glycosphingolipid receptors
739 with membrane microdomains of toxin-sensitive lymphoid and myeloid cells. *J*
740 *Lipid Res* 54(3):692–710.
741 20. Tesh VL (2013) Activation of Cell Stress Response Pathways By. 14(1):1–9.
742 21. Smith WE, et al. (2003) Shiga Toxin 1 Triggers a Ribotoxic Stress Response
743 Leading to p38 and JNK Activation and Induction of Apoptosis in Intestinal
744 Epithelial Cells. 71(3):1497–1504.
745 22. Jandhyala DM, et al. (2015) Activation of the Classical Mitogen-Activated Protein
746 Kinases Is Part of the Shiga. *Infect Immun* 84(1):138–148.
747 23. Blondel CJ, et al. (2016) CRISPR / Cas9 Screens Reveal Requirements for Host
748 Cell Sulfation and Fucosylation in Bacterial Type III Secretion System-Mediated
749 Cytotoxicity. *Cell Host Microbe* 20(2):226–237.
750 24. Tao L, et al. (2016) Frizzled proteins are colonic epithelial receptors for C. difficile
751 toxin B. *Nature* 538(7625):350–355.

752 25. Savidis G, et al. (2016) Identification of Zika Virus and Dengue Virus Dependency
753 Factors using Functional Genomics. *Cell Rep* 16(1):232–246.
754 26. Doench JG, et al. (2016) Optimized sgRNA design to maximize activity and
755 minimize off-target effects of CRISPR-Cas9. *Nat Biotechnol* 34(2):184–191.
756 27. Yamaji T, Hanada K (2015) Sphingolipid Metabolism and Interorganellar
757 Transport: Localization of Sphingolipid Enzymes and Lipid Transfer Proteins.
758 *Traffic* 16(2):101–122.
759 28. Tanaka A, et al. (2017) Genome-Wide Screening Uncovers the Significance of N-
760 Sulfation of Heparan Sulfate as a Host Cell Factor for Chikungunya Virus
761 Infection. *J Virol* 91(13):e00432-17.
762 29. Perrin J, et al. (2015) The nonaspanins TM9SF2 and TM9SF4 regulate the
763 plasma membrane localization and signalling activity of the peptidoglycan
764 recognition protein PGRP-LC in Drosophila. *J Innate Immun* 7(1):37–46.
765 30. Perrin J, et al. (2015) TM9 family proteins control surface targeting of glycine-rich
766 transmembrane domains. *J Cell Sci* 128(13):2269–2277.
767 31. Hogue DL, Nash C, Ling V, Hobman TC (2002) Lysosome-associated protein
768 transmembrane 4 alpha (LAPTM4 alpha) requires two tandemly arranged
769 tyrosine-based signals for sorting to lysosomes. *Biochem J* 365(Pt 3):721–30.
770 32. Grabner A, et al. (2011) LAPTM4A interacts with hOCT2 and regulates its
771 endocytotic recruitment. *Cell Mol Life Sci* 68(24):4079–4090.
772 33. Foster GH, Armstrong CS, Sakiri R, Tesh VL (2000) Shiga toxin-induced tumor
773 necrosis factor alpha expression: requirement for toxin enzymatic activity and
774 monocyte protein kinase C and protein tyrosine kinases. *Infect Immun*

68(9):5183–5189.

34. Milkereit R, Rotin D (2011) A role for the ubiquitin ligase Nedd4 in membrane sorting of LAPTM4 proteins. *PLoS One* 6(11):3–4.

35. Fleischmann KK, Pagel P, Schmid I, Roscher AA (2014) RNAi-mediated silencing of MLL-AF9 reveals leukemia-associated downstream targets and processes. *Mol Cancer* 13(1):1–14.

36. Wei J, et al. (2017) Overexpression of transcription factor activating enhancer binding protein 4 (TFAP4) predicts poor prognosis for colorectal cancer patients. *Exp Ther Med* 14(4):3057–3061.

37. Thollet A, et al. (2010) ZNF217 confers resistance to the pro-apoptotic signals of paclitaxel and aberrant expression of Aurora-A in breast cancer cells. *Mol Cancer* 9:291.

38. Furukawa T, Sunamura M, Motoi F, Matsuno S, Horii A (2003) Potential tumor suppressive pathway involving DUSP6/MKP-3 in pancreatic cancer. *Am J Pathol* 162(6):1807–1815.

39. Hayward RD, et al. (2005) Cholesterol binding by the bacterial type III translocon is essential for virulence effector delivery into mammalian cells. *Mol Microbiol* 56(3):590–603.

40. Lafont F, Nhieu GT Van, Hanada K, Sansonetti P, Goot FG Van Der (2002) Initial steps of Shigella infection depend on the cholesterol / sphingolipid raft-mediated CD44 ± IpaB interaction. *EMBO J* 21(17):4449–4457.

41. van der Goot FG, Tran van Nhieu G, Allaoui A, Sansonetti P, Lafont F (2004) Rafts can trigger contact-mediated secretion of bacterial effectors via a lipid-

based mechanism. *J Biol Chem* 279(46):47792–47798.

42. Kojima Y, et al. (2000) Molecular cloning of globotriaosylceramide/CD77 synthase, a glycosyltransferase that initiates the synthesis of globo series glycosphingolipids. *J Biol Chem* 275(20):15152–15156.

43. Yamaji T, Hanada K (2014) Establishment of HeLa cell mutants deficient in sphingolipid-related genes using TALENs. *PLoS One* 9(2):e88124.

44. Yamaji T, Hanada K (2015) Sphingolipid metabolism and interorganellar transport: localization of sphingolipid enzymes and lipid transfer proteins. *Traffic* 16(2):101–122.

45. Sheahan KL, Isberg RR (2015) Identification of mammalian proteins that collaborate with type III secretion system function: involvement of a chemokine receptor in supporting translocon activity. *MBio* 6(1):1–13.

46. Jerse AE, Yu J, Tall BD, Kaper JB (1990) A genetic locus of enteropathogenic Escherichia coli necessary for the production of attaching and effacing lesions on tissue culture cells. *Proc Natl Acad Sci U S A* 87(20):7839–7843.

47. Crawford JA, Kaper JB (2002) The N-terminus of enteropathogenic Escherichia coli (EPEC) Tir mediates transport across bacterial and eukaryotic cell membranes. *Mol Microbiol* 46(3):855–868.

48. Kaper JB, Nataro JP, Mobley HLT (2004) Pathogenic Escherichia coli. *Nat Rev Microbiol* 2(2):123–140.

49. Kanack KJ, Crawford JA, Tatsuno I, Karmali MA, Kaper JB (2005) SepZ / EspZ Is Secreted and Translocated into HeLa Cells by the Enteropathogenic Escherichia coli Type III Secretion System. 73(7):4327–4337.

821 50. Hanashima T, et al. (2008) Effect of Gb3 in lipid rafts in resistance to Shiga-like
822 toxin of mutant Vero cells. *Microb Pathog* 45(2):124–133.
823 51. Legler DF, Doucey MA, Schneider P, Chapatte L, Bender FC BC (2005)
824 Differential insertion of GPI-anchored GFPs into lipid rafts of live cells. *Faseb J*
825 19(1):73–5.
826 52. Saslowsky DE, et al. (2013) Ganglioside GM1-mediated Transcytosis of cholera
827 toxin bypasses the retrograde pathway and depends on the structure of the
828 ceramide domain. *J Biol Chem* 288(36):25804–25809.
829 53. Baibakov B, Murtazina R, Elowsky C, Giardiello FM, Kovbasnjuk O (2010) Shiga
830 Toxin Is Transported into the Nucleoli of Intestinal Epithelial Cells via a Carrier-
831 Dependent Process. 1:1318–1335.
832 54. Sadiq SM, Hazen TH, Rasko DA, Eppinger M (2014) EHEC Genomics : Past ,
833 Present , and Future. *Microbiol Spectr* 2(3):1–13.
834 55. Sandvig K, van Deurs B (1996) Endocytosis, intracellular transport, and cytotoxic
835 action of Shiga toxin and ricin. *Physiol Rev* 76(4):949–966.
836 56. Lee SY, Lee MS, Cherla RP, Tesh VL (2008) Shiga toxin 1 induces apoptosis
837 through the endoplasmic reticulum stress response in human monocytic cells.
838 *Cell Microbiol* 10(3):770–780.
839 57. Cantarelli V V, et al. (2007) Tyrosine phosphorylation controls cortactin binding to
840 two enterohaemorrhagic Escherichia coli effectors: Tir and EspFu/TccP. *Cell*
841 *Microbiol* 9(7):1782–1795.
842 58. Vingadassalom D, et al. (2009) Insulin receptor tyrosine kinase substrate links the
843 E. coli O157:H7 actin assembly effectors Tir and EspF(U) during pedestal

844 formation. *Proc Natl Acad Sci U S A* 106(16):6754–6759.

845 59. Campellone KG, et al. (2008) Repetitive N-WASP-binding elements of the
846 enterohemorrhagic Escherichia coli effector EspF(U) synergistically activate actin
847 assembly. *PLoS Pathog* 4(10):e1000191.

848 60. Weiss SM, et al. (2009) IRSp53 links the enterohemorrhagic E. coli effectors Tir
849 and EspFU for actin pedestal formation. *Cell Host Microbe* 5(3):244–258.

850 61. Cabrita MA, Hobman TC, Hogue DL, King KM, Cass CE (1999) Mouse
851 Transporter Protein , a Membrane Protein That Regulates Cellular Multidrug
852 Resistance , Is Localized to Lysosomes 1. (1):4890–4897.

853 62. Pacheco AR, Sperandio V (2012) Shiga toxin in enterohemorrhagic E . coli :
854 regulation and novel anti-virulence strategies. 2(June):1–12.

855 63. Kavaliauskiene S, Dyvelingelem AB, Skotland T, Sandvig K (2017) Protection
856 against shiga toxins. *Toxins (Basel)* 9(2):1–25.

857 64. Zhou X, et al. (2013) Vibrio parahaemolyticus T3SS Effector Mediates
858 Pathogenesis by Independently Enabling Intestinal Colonization and Inhibiting
859 TAK1 Activation. *CellReports* 3(5):1690–1702.

860 65. Datsenko KA, Wanner BL (2000) One-step inactivation of chromosomal genes in
861 Escherichia coli K-12 using PCR products. *Proc Natl Acad Sci U S A*
862 97(12):6640–6645.

863 66. Munera D, et al. (2014) Autotransporters but not pAA are critical for rabbit
864 colonization by Shiga toxin-producing Escherichia coli O104:H4. *Nat Commun* 5.
865 doi:10.1038/ncomms4080.

866 67. Knutton S, Baldwin T, Williams PH, McNeish AS (1989) Actin accumulation at

sites of bacterial adhesion to tissue culture cells: basis of a new diagnostic test for enteropathogenic and enterohemorrhagic Escherichia coli. *Infect Immun* 57(4):1290–1298.

Figure Legends

Figure 1. Design of a CRISPR/Cas9 screen to identify host factors underlying susceptibility to EHEC infection. A) Schematic of the infection and outgrowth process for an HT-29 Cas9/CRISPR library undergoing multiple rounds of infection with Δ*espZ* EHEC, which has an active T3SS and secretes Stx1 and Stx2. B, C) Abundance of HT29 cells infected with the indicated strain relative to the abundance of mock-infected cells at day 1 (B) and day 5 (C) post-infection. Graphs display mean and SD from 3 independent experiments. P values (**P<0.01, ****P<0.0001)

Figure 2. Mutations that disrupt sphingolipid biosynthesis and poorly characterized genes are enriched in the HT-29 CRISPR/Cas9 library following repeated infection with *espZ* EHEC.

A) Scatterplot of the statistical significance in each library (A and B) associated with the genes ranked in the top 5% by the STARS algorithm. Genes with a p value <= 0.001 in both libraries (upper right quadrant) are named; genes within the ellipse all have p values $<2.0e^{-06}$. B) Products of genes shown in (A) with p<=0.001 in both libraries and schematic representation depicting the subcellular localization of enzymes (black) that contribute to sphingolipid biosynthesis. A subset of substrates/products are depicted in

red. C) Abundance of HT29 control and mutant cells infected with Δ*espZ* EHEC relative to the abundance of mock-infected cells at day 5 post infection. Graphs display mean and SD from 3 independent experiments compared to HT-29 Cas9 (leftmost bar). P values (* P<0.05, ** P<0.005, *** P<0.001, ****P<0.0001)

Figure 3. Disruption of host sphingolipid biosynthesis genes and poorly characterized genes reduces the activity and cytotoxicity of EHEC's T3SS. A) Abundance of control and mutant HT29 Cas9 cells infected with Δ*espZ* Δ*stx1* Δ*stx2* EHEC relative to the abundance of mock-infected cells at day 1 post infection. Graphs display mean and SD from 3 independent experiments. P values (* P<0.02, ** P<0.01, *** P < 0.001, **** P<0.0001) were obtained from one-way ANOVA with Dunnet post-correction. B) Relative translocation of Tir-CyA from wt EHEC into HT-29 Cas9 control cells and the indicated HT-29 mutants, based on cAMP levels. Translocation into HT-29 Cas9 control cells was set as 100%. Data reflect mean and SD from 3 independent experiments. P values (**** P<0.0001) are based on one-way ANOVA with Dunnet post-correction. C) Confocal microscopy of control and mutant HT-29 Cas9 cells infected for 6 hr with GFP-EHEC, then stained for F-actin with Alexa647-phalloidin (pink) and DAPI (blue; labels nuclei). Merged images are shown. Focal colocalization of bacteria and actin reflects formation of actin pedestals. White boxes show enlarged image, to highlight pedestals. D) Percentage of the indicated host cells with actin pedestals 6 hr after infection. 250 cells were assessed for each host genotype. E) Number of pedestals per host cell; box plots show range (min to max) of pedestal numbers. 100 cells with AE lesions were counted per genotype. P values (**** P<0.0001)

Figure 4. TM9SF2 and LAPTM4A promote sensitivity to Stx. A) Abundance of wt and mutant HT29 Cas9 cells infected with T3SS-deficient EHEC (Δ*espZ* Δ*escN)* relative to the abundance of mock-infected cells at day 5 post infection. P values (**** P<0.0001) are based on one-way ANOVA with Dunnet post-test correction. B) Flow cytometry analysis of Stx2-Alexa647 binding to wt and mutant HT-29 Cas9 cells. Histograms show the distribution of fluorescence intensity in the total cell population in the presence and absence of toxin. C, D) Confocal microscopy of Stx2-Alexa488 (green) binding to non-permeabilized (C) and permeabilized (D) control and mutant HeLa Cas9 cells. Cells were also stained with DAPI and Alexa568-phalloidin

Figure 5. Subcellular localization of TM9SF2, LAPTM4A and A4GALT in wt and mutant HeLa cells

A). Confocal immunofluorescence microscopy of HeLa cells stained with anti-TM9SF2 (A; green) anti-GM130 to label the Golgi (pink)and DAPI. For LAPTM4A localization, HeLa cells were transfected with GFP-tagged LAPTM4A which was imaged directly after counterstaining as above. B) Confocal immunofluorescence microscopy of control and mutant HeLa Cas9 cells labeled with anti-A4GALT antibody (pink), anti-58K (red; labels Golgi) and DAPI (blue, labels nuclei). GM130 and 58K stain similar populations of Golgi membranes and were used interchangeably to accommodate the primary antibodies of interest.

Supplemental Information captions

Figure S1. Cytoxicity and host cell survival associated with various EHEC strains and purified toxin. A) Graphs show the abundance of HT29 cells infected with the indicated strain relative to the abundance of mock-infected cells at day 1 post infection with EHEC strains. Data reflect the mean +/- SD (n=3). P values (* P<0.05, ** P<0.01, **** P<0.0001) **B)** Kinetics of HT-29 cell death and recovery after challenge with Δ*espZ* (red), the Shiga toxin-deficientΔ*espZ* Δ*stx1* Δ*stx2* (blue), the T3SS-deficient ΔespZ ΔescN (green), or mock infected. Data are representative of 3 independent experiments. C) Abundance of Shiga toxins 1 and 2 in media during infection of HT-29 cells with *ΔespZ* and *ΔespZΔstx1Δstx2* (negative control). Toxin levels were assayed at 3 hr post infection and at 6 hr post infection (3 hr post media change), using an ELISA with antibody 4D1 which detects both toxins. D) Survival of HT-29 cells after 6 hours intoxication with either pure Shiga toxin 1 or 2; UD = undetectable.

Figure S2. CRISPR screen results and validation of mutations generated in candidate loci. A) Box plots showing the distribution of sgRNA frequencies in each HT-29 CRISPR library prior to infection and following each round of infection with Δ*espZ* EHEC. Line in the middle of the box indicates the median and whiskers comprise the 5th to 95th percentile. B) Heatmap of sgRNA enrichment in each HT-29 CRISPR library after successive rounds of Δ*espZ* EHEC infection. The heatmap shows each of the 4 sgRNAs targeting the genes; the darkness of the blue color correlates with the fold-enrichment of the sgRNA compared to the input libraries. **C)** Western blot of whole cell lysates of HT-29 Cas9 cells and CRISPR mutants. Arrows indicate the molecular weight

corresponding to each target protein. Antibodies used for validation are listed in Table S4. **D**) Analysis of indels in HT-29 mutants. Trace files show sequence reads indicating gene disruption at the sgRNA binding site on A4GAL and LAPTM4A mutants, compared to the gene in the parental cell line (WT). Red box outlines the sgRNA sequence.

Figure S3. A) Single channel and merged images corresponding to merged images shown in Fig 3C generated from confocal microscopy of control and mutant HT-29 Cas9 cells infected for 6 hr with GFP-producing EHEC, then stained with Alexa-647-phalloidin and DAPI. Arrows in merged images indicate pedestals (arrow). B) Graphs show the abundance of HT29 cells infected with the indicated EPEC strain relative to the abundance of mock-infected cells 4hr-post-infection with EPEC. Data reflect the mean +/- SD (n=3). P values (* $P<0.05$, ** $P<0.01$, # $P<0.0001$) C) Abundance of control and mutant HT29 Cas9 cells infected with *espZ* and *escN* EPEC relative to the abundance of mock-infected cells at 4 hr post-infection. Data correspond to mean and SD from 3 independent experiments. P values (** $P<0.01$) D) Analysis of lipid rafts components in control and mutant HeLa cells. Representative confocal slice of adherent cell bottom, 24 hours after transfection with GFP-GPI which traffics to the plasma membrane and inserts preferentially into lipid rafts. E) Quantitation of lipid rafts in control HeLa Cas9 cells and mutants. Total plasma membrane fluorescence (arbitrary fluorescence units) is depicted, along with kinetics of fluorescence decay with quantitative photobleaching. Data represent mean/SEM.

Figure S4. Flow cytometry analyses of toxin binding to control and mutant host cells. A) Flow cytometry analysis of Stx2-Alexa647 binding to control and mutant HeLa Cas9 cells. Histograms show HeLa cell population in the presence (pink) or absence (green) of toxin. B) Flow cytometry analysis of CT-Alexa647 binding to control and mutant HT-29 cells Histograms show HT-29 cell population in the presence (pink) and absence (green) of toxin.

Figure S5. Visualization and quantitative analysis of Golgi structure in control and mutant host cells. A) Confocal immunofluorescence microscopy of Golgi structure in control and mutant Hela Cas9 cells. Cis-medial Golgi (pink) were stained with anti-GM130, and nuclei (blue) were stained with DAPI. B) Confocal immunofluorescence microscopy of the trans-Golgi network (TGN) in control and mutant Hela Cas9 cells. TGN was stained with TGN46 (green) and nuclei (blue) were stained with DAPI. C) Quantitative analysis of TGN morphology in control and mutant Hela Cas9 cells, based on cell staining shown in (B). Distance of TGN from nuclei (left) and nominal TGN area (right) were determined for at least 20 cells.

Table S1. Primers used to construct EHEC EDL933 mutants

Table S2. STARS analysis of Library B round 4

Table S3. Sequence of sgRNAs and plasmids used to construct HT-29 Cas9 and HeLa Cas9 CRISPR mutants

Table S4. Antibodies used for western blot and immunofluorescence

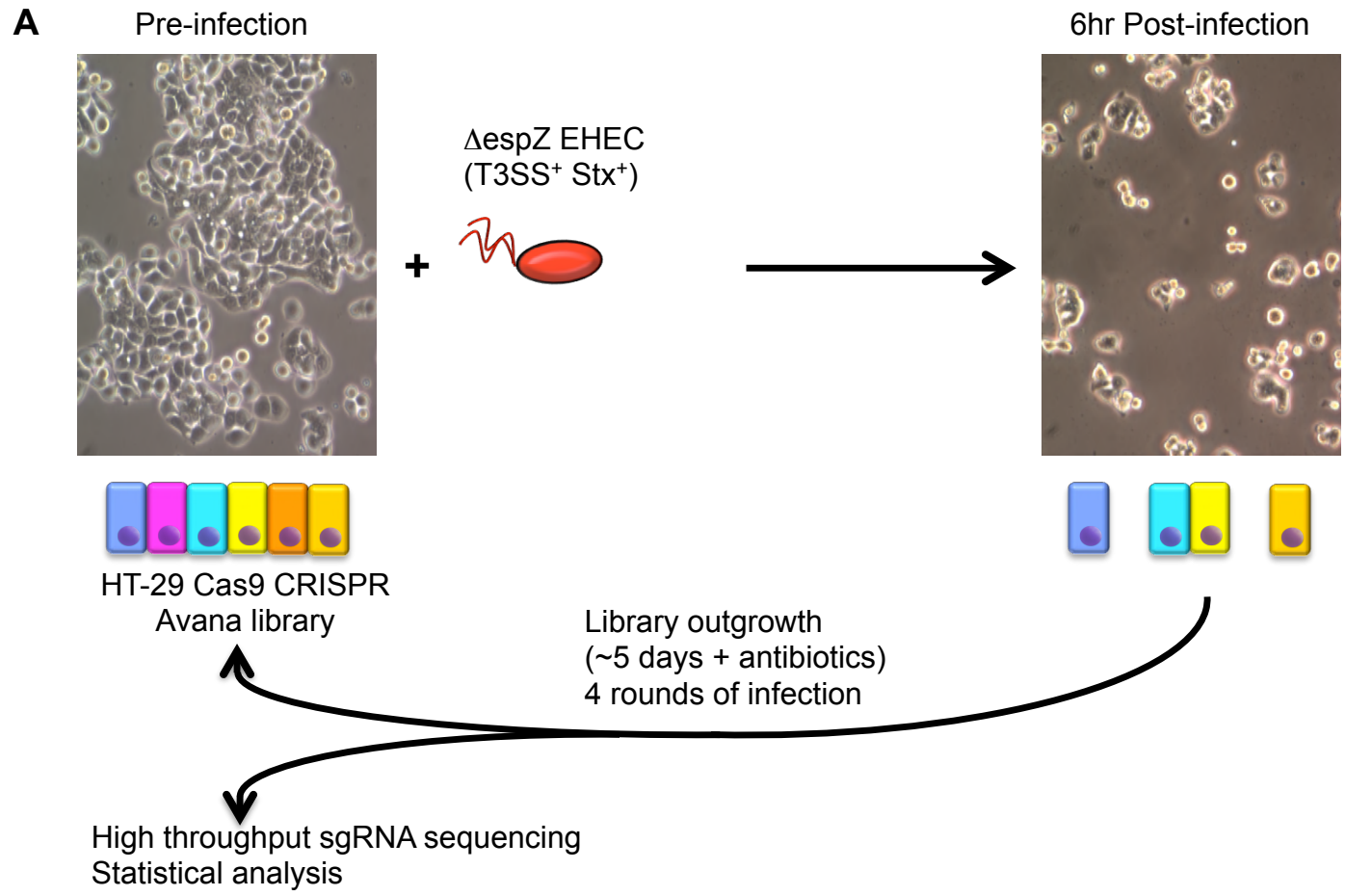

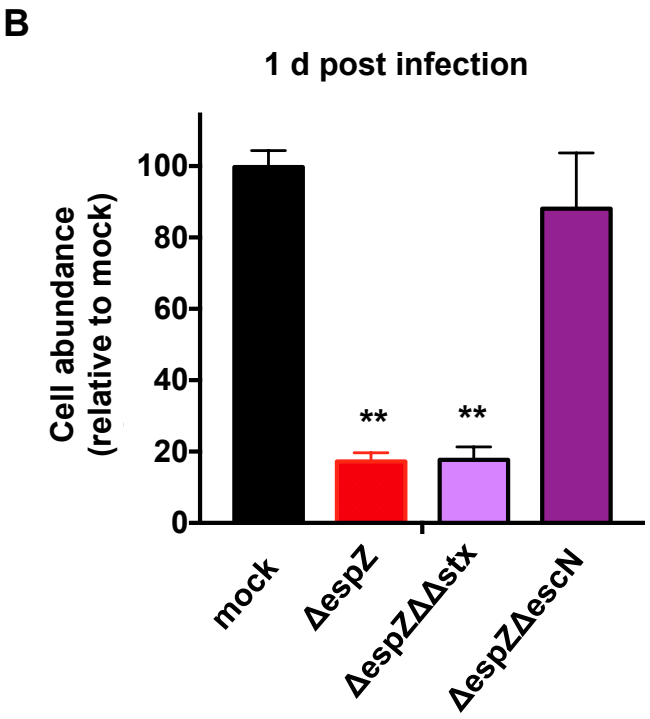

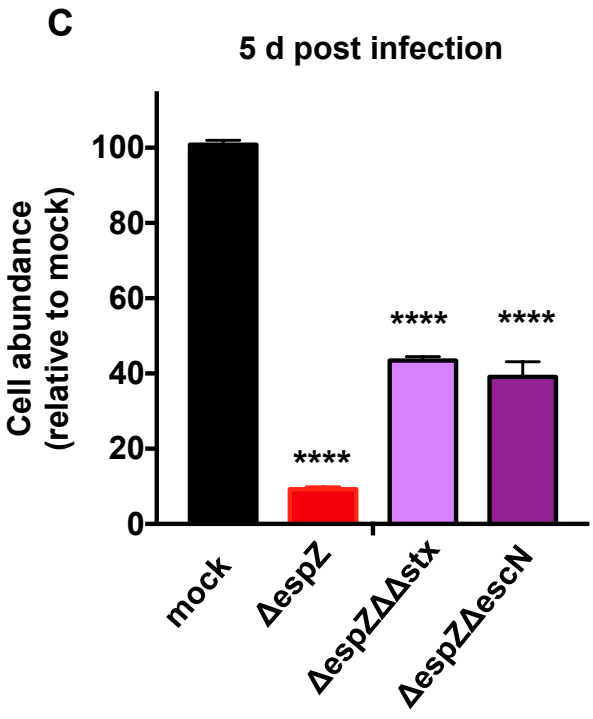

A

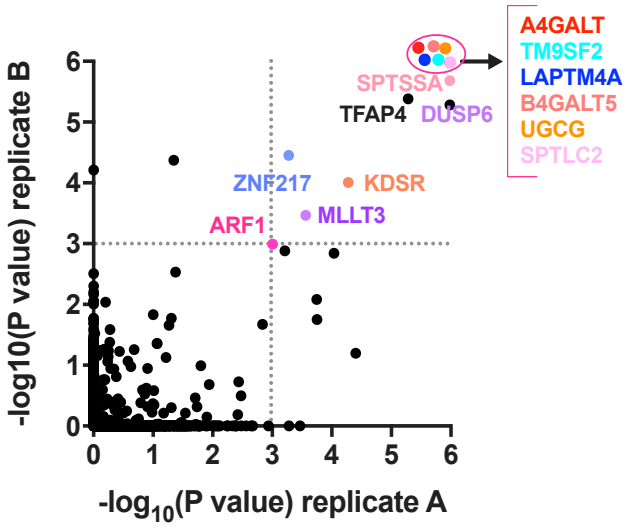

C

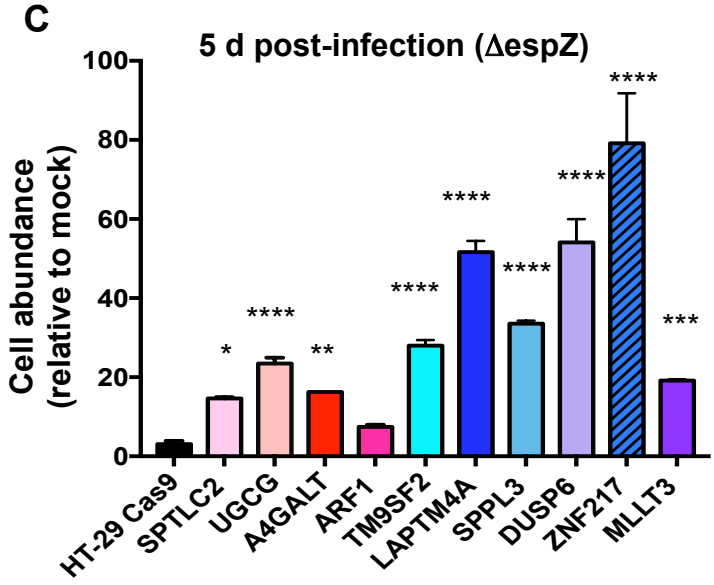

B

	Hit	Gene name
Sphingolipid biosynthesis	A4GALT	α-1,4-galactosyltransferase; Gb3 synthase
	B4GALT5	β-1,4-galactosyltransferase; major lactosylceramide synthase
	UGCG	UDP-glucose:ceramide glucosyltransferase; synthesize glucosylceramide
	KDSR	3-ketodihydrosphingosine reductase
	SPTLC2	serine palmitoyltransferase long chain base subunit 2
	SPTSSA	serine palmitoyltransferase small subunit A
	ARF1	ADP-ribosylation factor 1
Unknown	LAPTM4A	Lysosomal Protein Transmembrane 4 Alpha
	TM9SF2	Transmembrane 9 Superfamily Member 2
Cell proliferation	DUSP6	Dual Specificity Phosphatase 6; inactivates specifically ERK1/2
	TFAP4	Transcription Factor AP-4
	ZNF217	Zinc Finger Protein 217
	MLLT3	Myeloid/Lymphoid Or Mixed-Lineage Leukemia; Translocated To 3